Optics Letters

Filter width affects the transmittance of patterned all-dielectric Fabry–Perot filters: supplement

THOMAS GOOSSENS [ID]

Stanford Center for Image Systems Engineering, Stanford University, Stanford, California 94305, USA
(contact@thomasgoossens.be)

Filter width affects the transmittance of patterned all-dielectric Fabry-Perot filters: Supplemental document

CONTENTS

1. INTRODUCTION

This document contains supplementary derivations and additional documentation on experiments en simulations.

2. TRANSMITTANCE OF A 2D TINY FILTER USING AN ANGULAR SPECTRUM APPROACH

In this section the transmittance of a pixel-integrated (tiny) filter is calculated using an angular spectrum approach. The derivation in this chapter is original work but inspired on a derivation for the flux transfer of a wave-packet [1, p.70], also used for small-spot illumination calculations.

The novelty in this supplementary document is to limit the domain of integration to the size of the pixel which requires non-trivial modifications for practical computation. We will concern ourselves only with the *tangential* components of the field amplitudes as only these components contribute to flux transfer.

But first, for completeness of notation, the thin-film transfer-matrix is briefly introduced in Section A.

A. Thin-film transfer-matrix method for plane waves

For the case of plane-wave illumination on an infinitely wide filter there exists the well-known *transfer-matrix method* to calculate the transmittance [1, 2]. As conventional in the thin-film filter literature, we only consider the (complex-valued) electrical and magnetic field components that are parallel (tangential) to the thin-film filter surface, as only these components contribute to flux transfer across the interface [2].

For plane waves, we have that the tangential electrical field $\mathcal{E}$ and the magnetic field $\mathcal{H}$ are related as $\mathcal{H} = \eta E$, where η [$\mathrm{AV^{-1}}$] is the characteristic admittance of the medium. For the tangential

components, by construction, the characteristic admittance depends on the polarization and can be calculated as

$$\eta = \begin{cases} \dfrac{1}{\chi_0 \mu_r} \dfrac{n}{\cos \theta_n} & \text{p-polarized (TM)} \\[2ex] \dfrac{1}{\chi_0 \mu_r} n \cos \theta_n & \text{s-polarized (TE)} \end{cases}, \tag{S1}$$

with $\chi_0 = \sqrt{\mu_0/\epsilon_0} = 2.6544 \times 10^{-3}\,\text{S}$ defined as the admittance of free space [2] and θ_n the angle of refraction in the film, calculated using Snell's law. For optical frequencies $\mu_r \approx 1$ [2]. The polarization-dependent cosines are a direct consequence of mapping the actual field amplitudes onto the axis tangential to the material interface.

For multi-layer filters, one can define an equivalent admittance at each material interface, called the complex surface admittance $Y_j = \mathcal{H}_j / \mathcal{E}_j$ which can be calculated using the recurrence relation

$$Y_{j-1} = \frac{Y_j \cos \delta_j - i\eta_j \sin \delta_j}{\cos \delta_j - i\dfrac{Y_j}{\eta_j} \sin \delta_j}, \quad \text{for } j = N, \ldots, 0, \tag{S2}$$

with Y_0 being the surface admittance of the whole filter stack [1, p.123]. As there is no backward propagating wave in the substrate, $Y_{N-1} = \eta_N$, which can be used to initiate the recursion. Here, $\delta_i = \frac{2\pi n_i h_i \cos(\theta_i)}{\lambda}$ corresponds to the phase thickness of each layer.

In [1, p.126] it is then derived that for a thin-film filter stack, the transmission coefficient *for the tangential components* becomes

$$t = \frac{1 + r}{\prod_{j=1}^{p} (\cos \delta_j - i\frac{Y_j}{\eta_j} \sin \delta_j)}, \quad \text{with } r = \frac{\eta_0 - Y_j}{\eta_0 + Y_j}, \tag{S3}$$

which is constructed so that the transmitted plane wave in the substrate has an amplitude $\mathcal{E}_t = t\mathcal{E}_{\text{in}}$.

B. Tiny filter transmittance

The transmittance of a tiny filter is approximated as a small-spot illumination problem with a finite domain of integration on the bottom to include the finite size of the pixel. Because the number of generated electrons in the photodiode is proportional to the irradiance, the total pixel response effectively corresponds to an incoherent summation of the different parts of the outcoming wave front.

For a plane wave, a simple expression exists for the irradiance such that

$$I = \text{Re}(\eta)\frac{1}{2}\overline{\mathcal{E}}\mathcal{E}. \tag{S4}$$

For a wave packet, which consists of a distribution of plane waves, it is tempting to calculate the flux by summing up the irradiances for each plane wave in the decomposition. However, this approach would ignore the fact that the plane waves interfere.

In contrast, the irradiance of an arbitrary wave is calculated as

$$I(x) = \frac{\text{Re}(\overline{\mathcal{E}}\mathcal{H})}{2}, \tag{S5}$$

which is the amplitude of the Poynting vector perpendicular to the material interface.

The total flux across the tiny filter is then obtained by integrating over the filter area:

$$\Phi = \int_{-w/2}^{w/2} I(x)\mathrm{d}x. \tag{S6}$$

Since the incoming wave is a plane wave, we can substitute Eq. (S4) such that the incident flux equals

$$\Phi_{\text{in}} = \frac{\eta_{\text{in}}w}{2}, \tag{S7}$$

a calculation which is not possible for the transmitted wave-packet.

To solve Eq. (S6) for a wave packet we make use of two identities. First, for an arbitrary wave packet consisting of plane waves, we can write

$$\mathcal{E}(x) = \int_{-\infty}^{\infty} A(\nu)e^{i(2\pi\nu x)}\mathrm{d}\nu, \tag{S8}$$

and

$$\mathcal{H}(x) = \int_{-\infty}^{\infty} B(\nu')e^{i(2\pi\nu' x)}\,\mathrm{d}\nu'\,. \tag{S9}$$

Second, for each plane wave, the magnetic field is related by the admittance η to the electrical field as $B(\nu') = \eta(\nu')A(\nu')$. The admittance is polarization and angle-dependent, and hence different for each plane wave in the decomposition. Its angle-dependency is encoded by its dependency on the spatial frequency ν'.

So we have that

$$\mathcal{H}(x) = \int_{-\infty}^{\infty} \eta(\nu')A(\nu')e^{i(2\pi\nu' x)}\,\mathrm{d}\nu'\,, \tag{S10}$$

which after substitution in Eq. (S6) gives

$$\Phi = \frac{1}{2}\mathrm{Re}\left(\int_{\nu}\int_{\nu'}\mathrm{d}\nu\mathrm{d}\nu'\overline{A(\nu)}\eta(\nu')A(\nu')\int_{-w/2}^{w/2}\mathrm{d}xe^{2i\pi(\nu'-\nu)x}\right). \tag{S11}$$

To speed up numerical integration and reduce required memory, several identities are used to reduce the number of integrals. First, we notice that the inner integral is a Fourier transform and solve it exactly so that

$$\begin{aligned}\Phi =& \frac{1}{2}\mathrm{Re}\left(\int_{\nu}\int_{\nu'}\mathrm{d}\nu\mathrm{d}\nu'\overline{A(\nu)}\eta(\nu')A(\nu')\frac{\sin(\pi(\nu'-\nu)w)}{\pi(\nu'-\nu)}\right),\\ =& \frac{1}{2}\mathrm{Re}\left(\int_{\nu'}\mathrm{d}\nu'\eta(\nu')A(\nu')\int_{\nu}\mathrm{d}\nu\overline{A(\nu)}\frac{\sin(\pi(\nu'-\nu)w)}{\pi(\nu'-\nu)}\right).\end{aligned} \tag{S12}$$

Second, the new inner integral is in fact a convolution integral such that we can write

$$\Phi = \frac{1}{2}\mathrm{Re}\left(\int_{\nu'}\mathrm{d}\nu'\eta(\nu')A(\nu')(\overline{A}*K)(\nu')\right), \tag{S13}$$

with

$$K(\nu') = \frac{\sin(\pi\nu'w)}{\pi\nu'}, \tag{S14}$$

which I refer to as the "pixel kernel" in the software implementations. When necessary, the convolution can be computed efficiently in $O(n\log n)$ time using a Fast-Fourier Transform (FFT).

The transmitted flux becomes

$$\Phi_{\mathrm{t}} = \frac{1}{2}\mathrm{Re}\left(\int_{\nu'}\mathrm{d}\nu'\eta_{\mathrm{t}}(\nu')A_{\mathrm{t}}(\nu')(\overline{A_{\mathrm{t}}}*K)(\nu')\right). \tag{S15}$$

We can limit the integration domain to the incident wave between $\pm 90°$ incidence such that the limits of the domain are

$$\nu = \pm\frac{1}{\lambda}. \tag{S16}$$

Finally, we have that the transmittance of a tiny filter equals

$$T(\lambda;\theta) = \frac{\Phi_{\mathrm{t}}}{\Phi_{\mathrm{in}}}. \tag{S17}$$

3. DIFFERENCE BETWEEN TINY FILTER AND INFINITE FILTER WITH FINITE COLLECTION AREA

In this section it is shown the size of the collection area, i.e. pixel, is irrelevant for an infinite filter. This demonstrates an important qualitative difference between a finite filter and infinite filters.

For an infinite filter, the incident field is a plane wave:

$$\mathcal{E}_{\text{in}}(x) = \underbrace{e^{2\pi i x \sin\theta/\lambda}}_{\text{Plane wave}}, \tag{S18}$$

with an angular spectrum

$$A_{\text{in}}(\nu) = \int_{-\infty}^{+\infty} \mathcal{E}_{\text{in}}(x)e^{-i(2\pi\nu x)}\mathrm{d}x = \delta\left(\nu - \frac{\sin\theta}{\lambda}\right), \tag{S19}$$

such that the transmitted field equals

$$A_{\text{t}}(\nu) = t(\nu)A_{\text{in}}(\nu), \tag{S20a}$$

with t the transmission coefficient obtained using the transfer matrix method (see Eq. (S3)).

The flux transmitted through a finite area for an arbitrary angular spectrum equals (see Eq. (S11))

$$\Phi_{\text{t}} = \frac{1}{2}\int_{\nu}\int_{\nu'}\mathrm{d}\nu\mathrm{d}\nu'\overline{A_{\text{t}}(\nu)}\eta_{\text{t}}(\nu')A_{\text{t}}(\nu')\int_{-w/2}^{w/2}\mathrm{d}x\,e^{2i\pi(\nu'-\nu)x}, \tag{S21}$$

and the incident flux equals

$$\Phi_{\text{in}} = \frac{1}{2}\int_{\nu}\int_{\nu'}\mathrm{d}\nu\mathrm{d}\nu'\overline{A_{\text{in}}(\nu)}\eta_{\text{in}}(\nu')A_{\text{in}}(\nu')\int_{-w/2}^{w/2}\mathrm{d}x\,e^{2i\pi(\nu'-\nu)x}. \tag{S22}$$

Substituting Eq. (S19) into the flux formula and using the sampling property of the Dirac delta distribution, we obtain

$$\begin{aligned}
\Phi_{\text{in}} &= \frac{1}{2}\eta_{\text{in}}(\nu_\theta)\int_{-w/2}^{w/2}\mathrm{d}x\,\underbrace{e^{2i\pi(\nu_\theta-\nu_\theta)x}}_{=1}, \\
&= \frac{1}{2}\eta_{\text{in}}(\nu_\theta)w,
\end{aligned} \tag{S23}$$

with $\nu_\theta = \dfrac{\sin\theta}{\lambda}$.

Equivalently, we obtain for the transmitted flux that

$$\Phi_{\text{t}} = \frac{1}{2}\eta_{\text{t}}(\nu_\theta)w\overline{t(\nu_\theta)}t(\nu_\theta). \tag{S24}$$

So finally, if we calculate the effective transmittance for an infinite filter with a finite collection area we obtain

$$T = \frac{\Phi_{\text{t}}}{\Phi_{\text{in}}} = \frac{\eta_{\text{t}}(\nu_\theta)}{\eta_{\text{in}}(\nu_\theta)}\overline{t(\nu_\theta)}t(\nu_\theta) = T_\infty \tag{S25}$$

which corresponds to the definition of transmittance for a regular infinite filter (for real values of η) [1, p.132].

A possible intuitive explanation goes as follows. A Fabry-Perot filter requires light beams in the cavity to reflect many times and interfere with other parts of the beam in cavity. This essentially corresponds to a converging summation of a mathematical series [3]. For an infinitely wide filter with a finite collection area, although the collection area is finite, there remain an infinite number interfering contributions that arrive from outside of the collection area by traveling through the infinitely wide cavity. Hence, the series still converges. In contrast, for a tiny filter, while the collection area is equally large, there is no supply of interfering beams coming from outside this area and hence the sum is truncated, causing a deterioration of filter quality. In future work it would be interesting to further formalize this, for example, using the approach presented in [3].

4. RELATIONSHIP BETWEEN NORMALIZED FWHM AND MIRROR REFLECTANCE

A key property of the equivalent monolayer model is that its response is fully determined by two dimensionless factors, the effective refractive index n_{eff} and the reflectance R of the mirrors. In this section it is shown that the mirror reflectance determines the filter bandwidth normalized by its central wavelength. I present my own derivation because I believe it to more explicit about the assumptions than the derivations I found in reference works like [4, p.365] and [2, p.185].

Let us consider the transmittance for an infinitely wide filter of unit peak value so that

$$T_{\text{peak}} = \frac{(1-R)^2}{R^2 - 2R\cos(2\delta) + 1}. \tag{S26}$$

The goal is to find the phase thickness for which the peak transmittance is halved (equals $1/2$). Solving to δ we obtain

$$\delta_{1/2} = \frac{1}{2}\arccos\left(2 - \frac{R}{2} - \frac{1}{2R}\right). \tag{S27}$$

To find the FWHM, we need to derive how a change in phase-thickness translates to a change in wavelength. The phase thickness is non-linearly related to the wavelength as

$$\delta = \frac{2\pi n_{\text{eff}} h_{\text{eff}}}{\lambda} = \frac{\pi \lambda_{\text{cwl}}}{\lambda}, \tag{S28}$$

which can be differentiated such that

$$\mathrm{d}\delta = -\frac{\pi \lambda_{\text{cwl}}}{\lambda^2}\,\mathrm{d}\lambda. \tag{S29}$$

In the neighborhood of the central wavelength $\lambda = \lambda_{\text{cwl}}$ this gives

$$\mathrm{d}\delta = -\frac{\pi\,\mathrm{d}\lambda}{\lambda_{\text{cwl}}}. \tag{S30}$$

Assuming this equation holds for well for small enough finite ranges, we have that for $\Delta\delta = |2\delta_{1/2}|$,

$$\Delta\delta \approx \pi\frac{\text{FWHM}}{\lambda_{\text{cwl}}} = \pi\Lambda_\infty \tag{S31}$$

with

$$\Lambda_\infty = \frac{\text{FWHM}}{\lambda_{\text{cwl}}}. \tag{S32}$$

the normalized bandwidth of the corresponding infinitely wide filter at normal incidence.

After substitution, we obtain the expression for the normalized filter bandwidth

$$\Lambda_\infty \quad \approx \quad \frac{1}{\pi}\arccos\left(2 - \frac{R}{2} - \frac{1}{2R}\right), \tag{S33a}$$

$$\sim \quad \frac{1-R}{\pi\sqrt{R}}, \text{ for } R \to 1, \tag{S33b}$$

$$\sim \quad \frac{1-R}{\pi}, \text{ for } R \to 1, \tag{S33c}$$

which can also be solved to R such that

$$R \quad = \quad 2 - \cos(\pi\Lambda_\infty) - \sqrt{3 - 4\cos(\pi\Lambda_\infty) + \cos^2(\Lambda_\infty \pi)},$$
$$\sim \quad 1 - \pi\Lambda_\infty, \text{ for } \Lambda_\infty \to 0. \tag{S34}$$

While this approximation is very good for narrowband filters, the analysis is simpler in the wavenumber domain because the wavenumber and phase thickness are linearly related. Hence no approximation is required to relate the wavenumber-FWHM to the mirror reflectance so that

$$\delta = \frac{\pi k}{k_{\text{cwl}}} \Rightarrow \Delta\delta = \pi\frac{\Delta_k}{k_{\text{cwl}}}, \tag{S35}$$

5

and

$$\frac{\Delta k}{k_{cwl}} = \frac{1}{\pi} \arccos\left(2 - \frac{R}{2} - \frac{1}{2R}\right). \tag{S36}$$

In this work I opted to work in the wavelength domain because it is most familiar to the target audience.

5. ADDITIONAL DETAILS FOR THE NUMERICAL FDFD SIMULATION

The wave-optics method is validated by solving Maxwell's equations using a finite-difference frequency-domain (FDFD) Matlab Toolbox [5]. The frequency domain toolbox, used with a direct solver, is used for two reasons. First, we are only interested in the harmonic regime and hence time steps are not required. Second, the toolbox is very convenient for define rectangular structures like thin-film filters.

Three different Fabry-Pérot filters are placed adjacently as in Fig. S1. Each filter has a standard all-dielectric Fabry-Perot design [2]:

$$\text{Air}|H(LH)^b|L_c|(HL)^bH|\text{Substrate}, \tag{S37}$$

where each layer is a quarter-wave plate for a chosen wavelength and LH indicates a layer of low and then high refractive index. The exponent in $(LH)^b$ indicates this pattern is repeated b times. The three designs are

$$\begin{aligned} \text{Left}: \quad & \text{Air}|H(LH)^4L_1L(HL)^4H|\text{Substrate} \\ \text{Central}: \quad & \text{Air}|H(LH)^4LL(HL)^4H|\text{Substrate} \\ \text{Right}: \quad & \text{Air}|H(LH)^4L_3L(HL)^4H|\text{Substrate} \end{aligned} \tag{S38}$$

Where L and H are quarter-wave layers for a central wavelength around $\lambda_{cwl} = 720$ nm. By construction, this means that the dielectric mirror has a central wavelength around 720 nm. The material parameters that were used are $n_{air} = 1$, $n_l = 1.5$, $n_h = 2.4$, and $n_{sub} = 3.67$.

The central wavelength of the filter can be chosen by varying the cavity thickness. By choosing layers L_1 and L_3 to be 50 nm thinner and thicker than L respectively we obtain central wavelengths for the left, central, and right filter of 664 nm, 720 nm, and 776 nm respectively. These were chosen to be far enough such that there is no spectral overlap and cross-talk can be, supposedly, ignored.

The grid size is 6 nm and the perfectly matched layers (PML) are 100 nm on each border. In addition, an s-polarized plane wave source is placed above the filters. The simulation domain is visualized in Fig. S1.

To ensure realistic boundary conditions only the the transmittance of the central filter is calculated. The incident flux is calculated in the absence of any filter and substrate. The transmitted power is calculated by integrating the the power flux across the width of the filter. Depth-dependent absorption in the pixel is not modeled as this work focuses on calculating how much light is transmitted to the pixel, not modeling its quantum efficiency.

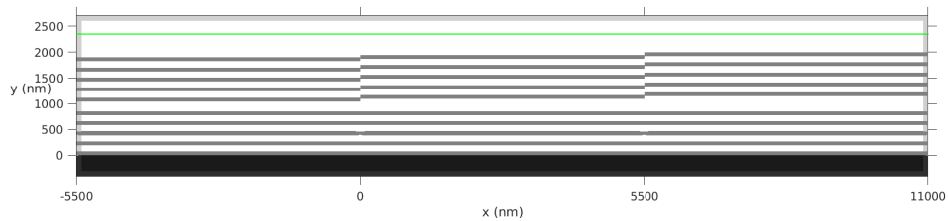The script for this simulation is available as Supplemental Code 1.

Fig. S1. FDFD simulation domain with three adjacent Fabry-Pérot filters on a single substrate.

6. CONTRIBUTION OF DIFFRACTION AT NORMAL INCIDENCE

The goal of this section is to estimate for which filter widths the diffraction effect at normal incidence becomes negligible. This requires us to define what "large" means given that the drop in peak transmittance will depend on multiple factors: the central wavelength λ_{cwl}, the normalized bandwidth Λ_{∞}, the effective refractive index n_{eff}, and the filter width w.

The strategy is to find a dimensionless parameter α which fully characterizes the peak drop $S(\alpha)$ and which is a function of all relevant system parameters so that

$$\text{peakvalue}(T_{\text{tiny}}^{\text{wave}}) = S(\alpha)\,\text{peakvalue}(T_{\infty}). \tag{S39}$$

This is the drop in peak transmittance due to diffraction in a tiny filter *relative* to the transmittance of the transmittance T_{∞} of an infinite filter (calculated using standard transfer-matrix calculations).

In Section A it is shown that for narrowband filters, i.e., $\Lambda_{\infty} \to 0$, the peak transmittance is fully characterized by the dimensionless parameter

$$\alpha = \Lambda_{\infty} \left(\frac{w n_{\text{eff}}}{\lambda_{\text{cwl}}} \right)^2. \tag{S40}$$

This means that, when plotted as a function of α, an identical drop in peak transmittance $S(\alpha)$ is observed for a wide range of filter designs (using the equivalent monolayer model). This result is demonstrated for several filter designs where the peak transmittances are plotted for a sweep of filter widths between 2 and 20 micron (Fig. S2). In addition, it was empirically found that

$$S(\alpha) = \frac{T_{\text{tiny}}^{\text{wave}}}{T_{\infty}} = \left(1 + \frac{3}{2\pi^2\alpha} \right)^{-1}. \tag{S41}$$

yields a good approximation of the scaling curves in Fig. S2. However, a rigorous asymptotic analysis would be interesting to perform in future work.

The larger the factor α, the smaller the peak drop caused by diffraction. Intuitively it makes sense that, the larger the width w is compared to the operating wavelength λ_{cwl}, the more negligible the effect of diffraction. Also, the larger the bandwidth Λ_{∞}, the more robust the filter spectrum for smoothing. Finally, the larger the effective refractive index n_{eff}, the smaller the angular sensitivity.

Thanks to the nondimensionalization, Fig. S2 captures with a single curve the effect of diffraction for narrowband filters. Hence, to determine for a given filter design what filter width should be considered small, one can calculate the corresponding α value and read the expected peak drop.
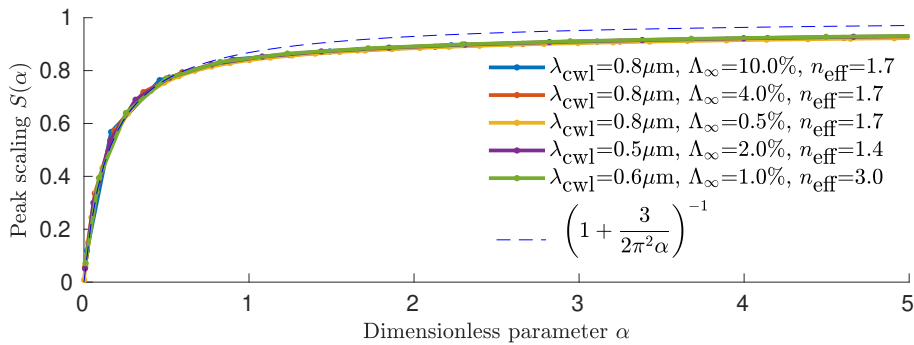

Fig. S2. Scaling $S(\alpha)$ of the peak transmittance for multiple filter designs. All curves are plot as a function of α at normal incidence.

A. Derivation of the dimensionless parameter for narrowband filters

In this section a derivation is presented to find the dimensionless parameter α used in the previous section. The derivation relies on the use of the equivalent monolayer model introduced in the

letter. We start from the transmitted flux integral (Eq. (S12)) which fully determines the shape of the transmittance. Here we only consider the case of normal incidence, i.e., $\theta = 0$, so that

$$\Phi_t = \frac{w^3}{2}\mathrm{Re}\left(\int_\nu \int_{\nu'} \overline{t(\nu)}t(\nu')\eta_t(\nu')\mathrm{sinc}\left(\pi w\nu\right)\mathrm{sinc}\left(\pi w\nu'\right)\mathrm{sinc}(\pi(\nu'-\nu)w)\mathrm{d}\nu\mathrm{d}\nu'\right). \tag{S42}$$

We shall also assume that in the small spatial frequency range of interest (which corresponds to small diffraction angles), the characteristic admittance can be considered η constant.

To place all width dependency of the integrand into the transmission functions, we make the substitutions $w\pi\nu = u$ and $w\pi\nu' = u'$ so that

$$\Phi_t = \frac{\eta_t}{2}w^3\mathrm{Re}\left(\iint\limits_{-\infty}^{\infty} \overline{t\left(\frac{u}{\pi w}\right)}t\left(\frac{u'}{\pi w}\right)\mathrm{sinc}(u)\mathrm{sinc}(u')\mathrm{sinc}(u'-u)\frac{\mathrm{d}u\mathrm{d}u'}{\pi^2 w^2}\right), \tag{S43}$$

$$= \frac{\eta_t}{2}\frac{w}{\pi^2}\mathrm{Re}\left(\iint\limits_{-\infty}^{\infty} \overline{t\left(\frac{u}{\pi w}\right)}t\left(\frac{u'}{\pi w}\right)\mathrm{sinc}(u)\mathrm{sinc}(u')\mathrm{sinc}(u'-u)\mathrm{d}u\mathrm{d}u'\right)$$

Because of this substitution, the value of the integral, and hence also the effect of diffraction, solely depends on the transmission function $t(\nu)$. In what follows we hence only have to examine the parameters that determine the shape of this transmission function. The derivation builds on the use of the transmission function of an equivalent monolayer. The facilitates an analysis in terms of general filter properties like its bandwidth, central wavelengths. The transmission coefficient of interest is derived in [4, p.362]

$$t(\delta) = \frac{t_s(1-R)}{1-Re^{i2\delta}}, \tag{S44}$$

and hence

$$L = \overline{t\left(\frac{u}{\pi w}\right)}t\left(\frac{u'}{\pi w}\right) = \frac{T_s(1-R)^2}{(1-Re^{-i2\delta})(1-Re^{i2\delta'})}, \tag{S45}$$

The transmission coefficient t_s only scales the integral function and is canceled out when normalizing by the infinite filter transmittance and can henceforth be ignored.

While L is a complex function, only its real part $L_r = \mathrm{Re}(L)$ (see Eq. (S5)) is important. One finds that

$$\begin{aligned}
L_r &= (1-R)^2\frac{(R^2\cos(2(\delta-\delta')) - R\cos(2\delta) - R\cos(2\delta') + 1)}{(R^2 - 2R\cos(2\delta) + 1)(R^2 - 2R\cos(2\delta') + 1)} \\
&\sim \frac{(1-R)^4}{(R^2 - 2R\cos(2\delta) + 1)(R^2 - 2R\cos(2\delta') + 1)}, \text{ for } \delta,\delta' \to \pi \\
&= l(\delta)l(\delta'),
\end{aligned} \tag{S46}$$

with

$$l(\delta) = \frac{(1-R)^2}{R^2 - 2R\cos(2\delta) + 1}, \tag{S47a}$$

$$\sim \frac{(1-R)^2}{R^2 - 2R(1 - 2(\delta-\pi)^2) + 1}, \delta \to \pi, \tag{S47b}$$

$$= \frac{(1-R)^2}{(1-R)^2 + 4R(\delta-\pi)^2} = \frac{\left(\frac{1-R}{2\sqrt{R}}\right)^2}{\left(\frac{1-R}{2\sqrt{R}}\right)^2 + (\delta-\pi)^2}, \tag{S47c}$$

$$= \frac{\left(\frac{\pi\Lambda_\infty}{2}\right)^2}{\left(\frac{\pi\Lambda_\infty}{2}\right)^2 + (\delta-\pi)^2}, \text{ (using Eq. (S33b)),} \tag{S47d}$$

$$= \frac{1}{1 + \frac{u^4}{\pi^4}\left(\frac{\lambda_{\mathrm{cwl}}^2}{w^2 n_{\mathrm{eff}}^2\Lambda_\infty}\right)^2} = \frac{1}{1 + \frac{u^4}{\pi^4\alpha^2}}, \text{ (See Section B),} \tag{S47e}$$

8

with

$$\alpha = \Lambda_\infty \left(\frac{w n_{\mathrm{eff}}}{\lambda_{\mathrm{cwl}}} \right)^2. \tag{S48}$$

Hence, we have reduced the characterization of the transmittance to a single dimensionless parameter. When this factor has the same value, the peak transmittance drop, relative to the infinite filter transmittance, also has to have same value.

B. Approximation of δ as a function of spatial frequency

In this section a useful approximation of the phase thickness δ is derived which is valid for small spatial frequencies (small angles) in the neighborhood of the main peak at normal incidence.

We start from the standard definition of phase thickness (see Eq. 5 in the main manuscript) so that

$$\delta = \frac{2\pi n_{\mathrm{eff}} h_{\mathrm{eff}} \cos(\theta_n)}{\lambda}. \tag{S49}$$

For small spatial frequencies this can be rewritten as

$$\delta \; = \; \frac{2\pi n_{\mathrm{eff}} h_{\mathrm{eff}} \cos(\theta_n)}{\lambda} = \frac{2\pi n_{\mathrm{eff}} h_{\mathrm{eff}} \sqrt{1 - \sin^2(\theta_n)}}{\lambda} \tag{S50a}$$

$$= \; \frac{2\pi n_{\mathrm{eff}} h_{\mathrm{eff}} \sqrt{1 - \dfrac{\sin^2(\theta_n)}{(\lambda/n_{\mathrm{eff}})^2}(\lambda/n_{\mathrm{eff}})^2}}{\lambda} \tag{S50b}$$

$$= \; \frac{2\pi n_{\mathrm{eff}} h_{\mathrm{eff}} \sqrt{1 - (\nu\lambda/n_{\mathrm{eff}})^2}}{\lambda} \, , \, \left(\text{using } \nu = \frac{\sin(\theta_n)}{\lambda/n_{\mathrm{eff}}} \right), \tag{S50c}$$

$$\sim \; \frac{2\pi n_{\mathrm{eff}} h_{\mathrm{eff}} \left(1 - \dfrac{\nu^2\lambda^2}{2n_{\mathrm{eff}}^2} \right)}{\lambda} \tag{S50d}$$

$$= \; \frac{2\pi n_{\mathrm{eff}} \overbrace{\left(\dfrac{\lambda_{\mathrm{cwl}}}{2n_{\mathrm{eff}}} \right)}^{h_{\mathrm{eff}}} \left(1 - \dfrac{\nu^2\lambda^2}{2n_{\mathrm{eff}}^2} \right)}{\lambda}. \tag{S50e}$$

To obtain the peak drop at the original peak wavelength λ_{cwl}, we set $\lambda = \lambda_{\mathrm{cwl}}$ so that

$$\delta \sim \frac{2\pi n_{\mathrm{eff}} \left(\dfrac{\lambda_{\mathrm{cwl}}}{2n_{\mathrm{eff}}} \right) \left(1 - \dfrac{\nu^2\lambda^2}{2n_{\mathrm{eff}}^2} \right)}{\lambda} = \pi \left(1 - \frac{\nu^2\lambda_{\mathrm{cwl}}^2}{2n_{\mathrm{eff}}^2} \right). \tag{S51}$$

Finally, applying the substitution $w\pi\nu = u$, we obtain the desired approximation

$$\delta \left(\frac{u}{\pi w} \right) = \pi \left(1 - \frac{u^2\lambda_{\mathrm{cwl}}^2}{w^2\pi^2 n_{\mathrm{eff}}^2} \right) = \pi - \frac{u^2\lambda_{\mathrm{cwl}}^2}{\pi w^2 n_{\mathrm{eff}}^2}. \tag{S52}$$

7. ADDITIONAL DETAILS ABOUT THE EXPERIMENTAL SETUP

A. Setup

The experimental setup consists of a monochromator coupled to a collimating lens which illuminates the sensor. The setup and its operation is described in [6]. Several components of the setup were updated but the operational principle remains unchanged. The image sensor board is placed onto a goniometer to control the incidence angle of the collimated light.

For each angle, this setup measures the spectral response of each pixel in digital numbers. The device under test is imec's snapshot 5x5 mosaic camera [7]. On this sensor, 25 filters are integrated on 5.5 µm wide pixels of a CMV2000 image sensor [8]. The filters are distributed across a wavelength range of 665 and 975 nm.

B. Fit at normal incidence

To apply the equivalent monolayer model to the measured data it was necessary to estimate the normalized bandwidth Λ_∞. This is the bandwidth of the filter at normal incidence, *if it were infinitely wide*, which is not known in this case. However, using the wave-optics model one can sweep across multiple bandwidths and use the tiny filter transmittance that best matches the measurement.

The result of this procedure is displayed for several filters in Fig. S3. The fit is not perfect for each filter because not each filter has a perfect Lorentzian shape.
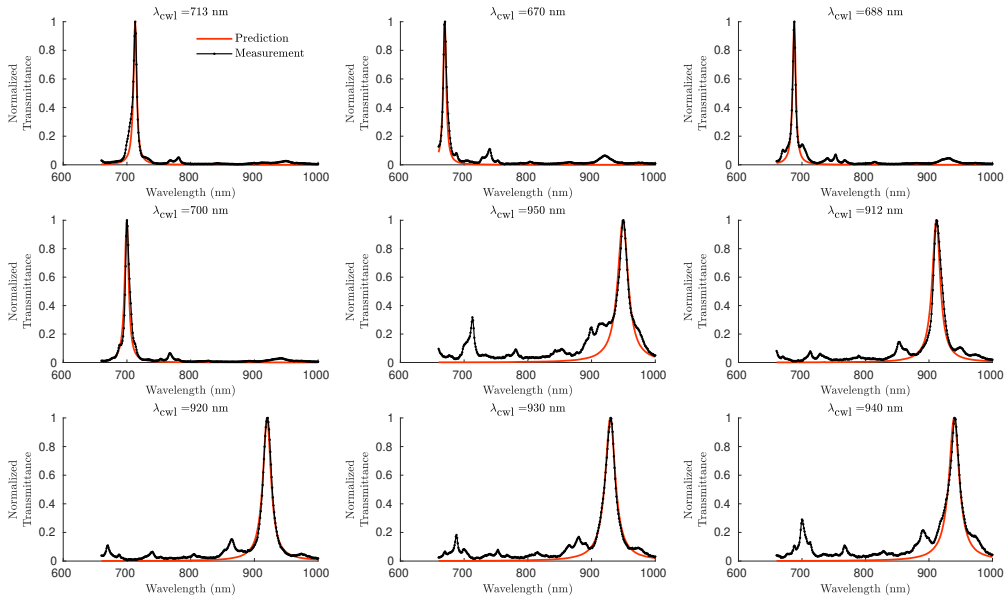

Fig. S3. Fit at normal incidence for several filters on imec's sensor.

REFERENCES

1. C. Amra, M. Lequime, and M. Zerrad, *Electromagnetic Optics of Thin-Film Coatings: Light Scattering, Giant Field Enhancement, and Planar Microcavities* (Cambridge University Press, 2021).
2. H. A. Macleod, *Thin-Film Optical Filters, Fifth Edition* (CRC press, 2017).
3. D. M. Marques, J. A. Guggenheim and P. R. T. Munro. (2021). "Analysing the impact of non-parallelism in Fabry-Perot etalons through optical modelling", Optics Express 29(14), 21603 (2021).
4. M. Born and E. Wolf, *Principles of Optics: Electromagnetic Theory of Propagation, Interference and Diffraction of Light* (Cambridge University Press, 1999), 7th ed.
5. W. Shin, "MaxwellFDFD Matlab toolbox, https://www.mit.edu/~wsshin/maxwellfdfd.html (Visited on March 2, 2021)." (2015).
6. P. Agrawal, K. Tack, B. Geelen, B. Masschelein, P. Mateo, A. Moran, A. Lambrechts, and M. Jayapala, "Characterization of VNIR Hyperspectral Sensors with Monolithically Integrated Optical Filters," Image Sensors Imaging Syst. pp. 1–7 (2016).
7. B. Geelen, N. Tack, and A. Lambrechts, "A compact snapshot multispectral imager with a monolithically integrated per-pixel filter mosaic," Proc. SPIE **8974**, 89740L (2014).
8. CMOSIS, "https://ams.com/cmv2000 (visited on 2021-03-02)." .